LAWRENCE
LIVERMORE
NATIONAL
LABORATORY

LLNL-JRNL-458115

Structural and optical properties of liquid CO2 up to 1 terapascal

B. Boates, S. Hamel, E. Schwegler, S. A. Bonev

October 4, 2010

Journal of Chemical Physics

Disclaimer

Structural and optical properties of liquid CO_2 up to 1 terapascal

B. Boates[1,2], S. Hamel[1], E. Schwegler[1], and S. A. Bonev[1,2]
[1] *Lawrence Livermore National Laboratory, P.O. Box 808 Livermore, California 94550*
[2] *Department of Physics, Dalhousie University, Halifax, NS, B3H 3J5, Canada*
(Dated: October 1, 2010)

We report on the use of first-principles molecular dynamics calculations to examine properties of liquid carbon dioxide in the pressure-temperature range of 0-1 TPa and 200-100,000 K. The computed equation of state points are used to predict a series of shock Hugoniots with initial starting conditions that are relevant to existing and ongoing shock-wave experiments. A comparison with published measurements up to 70 GPa shows excellent agreement. We find that the liquid undergoes a gradual phase transition along the Hugoniot and have characterized this transition based on changes in bonding and structural properties, as well as the conductivity and reflectivity of the fluid.

PACS numbers: 62.50.-p,02.70.-c,64.30.Jk, 61.20.Ja

I. INTRODUCTION

The properties of molecular solids and liquids as a function of pressure (P) and temperature (T) are of fundamental interest to a wide range of condensed matter physics and chemistry. In particular, molecular compounds based on the light *sp* valent elements C, N, and O often undergo pressure-induced ionization and polymerization transitions that can potentially lead to the formation of new materials with interesting properties [1, 2]. In addition, such compounds are thought to be important constituents of the Neptune-like ice planets [3–5].

The phase diagram of carbon dioxide has been recently the subject of intense interest. Most studies have focused on the crystalline phases up to $\sim$ 100 GPa and temperatures below 2000 K, where solid CO_2 undergoes polymerization transitions [1, 6–18]. To probe this regime experimentally, diamond anvil cell techniques have been utilized. The CO_2 phase diagram at higher pressure and temperature, and especially the liquid phases, has received much less attention. First-principles molecular dynamics simulations by Tassone *et al.* [19] were carried out near 50 GPa and 4000 K where evidence for the formation of short-lived C_2O_4 compounds was found. From the experimental side, the combination of extreme pressure *and* temperature can be readily achieved with shock-wave compression techniques. Such experiments have been performed using gas gun techniques to measure the CO_2 shock Hugoniot for pressures up to 70 GPa [20]. In these experiments, the Hugoniot curve appears to have a deflection near 40 GPa, indicating that CO_2 is likely undergoing a phase transition. To model a shock-induced dissociation transition above 34 GPa, a chemical model based on several gaseous species was introduced in [20], but the transition has not yet been examined using first-principles theory.

In this paper, we report on a series of first-principles equation of state (EOS) calculations of CO_2 that are in excellent agreement with existing gas gun measurements. Furthermore, we have extended the P-T range to 1 TPa and 100,000 K and have examined the effect of several initial density and temperature conditions. These results are relevant for ongoing and future experimental efforts. Due to the technical complexity of such experiments, their interpretation has sometimes proven to be challenging [21, 22]. In the past, theoretical calculations have played an important role in explaining and validating shock-wave measurements [23–29].

II. COMPUTATIONAL METHOD

A. First principles molecular dynamics

First-principles molecular dynamics (FPMD) simulations of carbon dioxide have been carried out for pressures up to 1 TPa using finite-temperature density functional theory (DFT) [30] within the Perdew-Burke-Ernzerhof generalized gradient approximation (PBE-GGA) [31] as implemented in $VASP$ [32]. The simulations were carried out in the canonical (NVT) ensemble using Born-Oppenheimer dynamics with a Nosé-Hoover thermostat. For each P and T, the system was equilibrated within 1-2 ps and simulated for over 10 ps using a 0.75 fs ionic time-step. Initially, all simulations were carried out with 32-molecule supercells, 4- and 6-electron projector augmented wave (PAW) pseudopotentials with 1.50 and 1.52 Bohr core radii for carbon and oxygen atoms, respectively, and a 500 eV plane-wave cut-off. For the P-T points closest to the Hugoniot (one for each density considered) the FPMD simulations were repeated with harder pseudopotentials - 1.10 Bohr core radii and 875 eV plane-wave cut-off. The resulting corrections to pressure, energy (E) and structure are minimal (exact P and E values given in the following section). Nevertheless, they have been incorporated into the Hugoniot calculations and all structural analysis presented in the paper is based on simulations with the harder pseudopotentials.

Additional convergence tests for finite size effects and

k-point Brillouin zone sampling were performed at several P-T conditions along the Hugoniot - before and after the dissociation transition, as well as at the highest pressures considered. These included: (i) FPMD simulations with 64-molecule supercells and the Γ **k**-point; (ii) FPMD simulations with 32-molecule supercells and a $2 \times 2 \times 2$ **k**-point grid; and (iii) static calculations with a $4 \times 4 \times 4$ **k**-point grid on 32-molecule liquid configurations. In all cases, changes in P, E, and the structure were negligible.

B. Optical properties

For temperature and density points close to the Hugoniot, the electronic conductivity was evaluated for 30 well spaced snapshots taken from the FPMD trajectory. The electrons and ions were assumed to be in local thermodynamical equilibrium with equal temperatures ($T_e = T_{ions}$) and the electronic temperature was used to determine the (possibly fractional) occupation number of the orbitals according to a Fermi distribution. Enough bands were used to obtain all excitations up to 80 eV. For each configuration drawn from the trajectories, the Γ-point electronic density from the MD was used to evaluate the set of Kohn-Sham orbitals at the $(\frac{1}{4}, \frac{1}{4}, \frac{1}{4})$ **k**-point (again using Fermi broadening at the ionic temperature). Based on these orbitals, the Kubo-Greenwood formula was used to estimate the real component of the frequency dependent conductivity [33, 34]:

$$\sigma(\omega) = \frac{2\pi e^2 \hbar^2}{3m^2\omega\Omega} \sum_{\mathbf{k}} W(\mathbf{k}) \sum_{j=1}^{N} \sum_{i=1}^{N} \sum_{\alpha=1}^{3} [F(\epsilon_{i,\mathbf{k}}) - F(\epsilon_{j,\mathbf{k}})] \times |\langle \Psi_{j,\mathbf{k}} | \nabla_\alpha | \Psi_{i,\mathbf{k}} \rangle|^2 \delta(\epsilon_{i,\mathbf{k}} - \epsilon_{j,\mathbf{k}} - \hbar\omega), \quad (1)$$

where e and m are the electron charge and mass, Ω is the cell volume, α denotes the x, y, and z directions, and $F(\epsilon_{i,\mathbf{k}})$ is the occupation number of the i'th eigenvalue at **k**-point **k**. The direct current (DC) conductivity is obtained as the zero frequency limit of $\sigma(\omega)$ averaged over the different configurations while the imaginary component of the conductivity is obtained by using the Kramers-Krönig transform:

$$\sigma_2(\omega) = -\frac{2}{\pi} P \int_0^\infty \frac{\sigma(\nu)\omega}{(\nu^2 - \omega^2)} d\nu \quad (2)$$

where P denotes the principal value of the integral. Using the complex conductivity, one can obtain the complex dielectric function ϵ, the index of refraction n, the coefficient of extinction k, and the reflectivity R:

$$\epsilon_1(\omega) = 1 - \frac{4\pi}{\omega}\sigma_2(\omega) \quad ; \quad \epsilon_2(\omega) = \frac{4\pi}{\omega}\sigma(\omega) \quad (3)$$

$$\epsilon(\omega) = \epsilon_1(\omega) + i\epsilon_2(\omega) = [n(\omega) + ik(\omega)]^2 \quad (4)$$

$$R(\omega) = \frac{[1 - n(\omega)]^2 + k^2(\omega)}{[1 + n(\omega)]^2 + k^2(\omega)} \quad (5)$$

III. RESULTS

A. Hugoniot

The specific EOS points that were used to interpolate the Hugoniot corresponding to an initial starting condition of liquid CO_2 at $\rho_0 = 1.172$ g/cc and $T_0 = 218.5$ K are provided in Table I. For each of the selected densities, the data can be readily used to accurately determine the pressure and temperature that satisfy the Hugoniot equation,

$$E - E_0 = \frac{1}{2}(P + P_0)(1/\rho - 1/\rho_0). \quad (6)$$

For this purpose, we used a linear interpolation of Eqn. 6 on a grid of temperatures. The results are directly compared with experimental measurements obtained by gas gun techniques in Fig. 1; the agreement with measured pressures and temperatures is excellent.

TABLE I: Pressure and internal energy of liquid CO_2 from FPMD simulations as a function of density and temperature. Uncertainties in the last digits are given in parentheses and are related to statistical averages of each simulation. Here dP and dE are the differences between the pressure and energy results obtained when using the 875 and the 500 eV pseudopotentials. For each density, these quantities were computed for one temperature, as indicated in the table. All remaining P and E values for the given density were corrected with the same dP and dE.

ρ(g/cc)	T(K)	P(GPa)	dP	E(eV/ion)	dE
1.172	218.5(4)	-0.125(4)	-0.36	-7.688(0.2)	-0.070
1.87	500(0.3)	4.52(1)	-0.73	-7.558(1)	-0.072
	1000(1)	5.67(3)		-7.424(1)	
	1500(1)	7.22(5)		-7.301(2)	
2.18	500(1)	11.0(0.3)		-7.484(1)	
	800(1)	12.1(1)		-7.400(1)	
	1000(1)	12.5(0.4)		-7.345(1)	
	1500(1)	14.3(0.4)	-0.35	-7.216(1)	-0.073
	2000(1)	16.1(1)		-7.092(1)	
2.36	500(1)	15.4(0.3)		-7.425(0.4)	
	1000(0.4)	17.3(1)		-7.286(1)	
	1500(1)	19.4(0.4)		-7.153(1)	
	2000(1)	21.1(1)		-7.024(2)	
	2500(1)	22.2(1)	-0.43	-6.900(2)	-0.076
2.57	1000(1)	23.8(1)		-7.208(1)	
	1500(1)	26.2(1)		-7.064(2)	
	2000(1)	27.8(1)		-6.936(2)	
	2500(1)	29.2(1)		-6.803(2)	
	3000(2)	31.0(2)		-6.678(2)	
	3500(2)	32.0(3)	-0.99	-6.534(3)	-0.081
2.80	2500(1)	39.9(4)		-6.697(3)	
	3000(1)	41.8(3)		-6.557(7)	
	3500(1)	42.6(2)		-6.412(6)	
	4000(2)	42.5(4)	-0.71	-6.212(7)	-0.113
	4500(2)	41.9(3)		-5.987(13)	
3.06	2500(2)	46.0(4)		-6.520(6)	
	3000(1)	49.1(5)		-6.313(4)	
	3500(1)	50.4(5)		-6.152(6)	
	4000(2)	51.0(5)		-5.973(8)	

ρ(g/cc)	T(K)	P(GPa)	dP	E(eV/ion)	dE
	4500(2)	51.6(4)		-5.783(13)	
	5000(2)	52.3(3)	0.02	-5.578(13)	-0.081
	5500(1)	53.2(2)		-5.388(9)	
3.35	3500(1)	60.1(5)		-5.960(5)	
	4000(2)	63.2(4)		-5.772(6)	
	4500(2)	65.1(5)		-5.572(11)	
	5000(2)	66.5(2)		-5.358(9)	
	5500(2)	68.6(3)		-5.154(10)	
	6000(2)	69.8(3)		-4.945(13)	
	6500(2)	72.2(3)		-4.764(14)	
	7000(2)	73.7(2)	0.02	-4.514(10)	-0.069
3.68	5000(2)	85.8(5)		-5.127(10)	
	5500(2)	88.3(4)		-4.901(14)	
	6000(2)	90.8(4)		-4.674(14)	
	6500(2)	93.7(4)		-4.467(10)	
	7000(2)	96.1(2)		-4.249(10)	
	7500(1)	98.6(2)		-4.055(12)	
	8000(3)	100.7(3)		-3.888(10)	
	8500(2)	103.8(2)		-3.686(8)	
	9000(2)	106.5(2)		-3.500(7)	
	9500(3)	108.9(3)		-3.309(13)	
	10000(2)	111.9(2)		-3.146(8)	
	18000(2)	156.2(1)		-0.736(6)	
	20000(2)	167.8(1)	-2.72	-0.162(4)	-0.050
4.05	10000(2)	150.8(3)		-2.843(9)	
	18000(2)	202.0(3)		-0.430(4)	
	20000(3)	215.3(2)		0.141(4)	
	22000(2)	228.1(2)		0.706(5)	
	24000(5)	240.9(2)		1.285(4)	
	26000(3)	253.8(2)		1.868(4)	
	70000(20)	554.9(8)	-0.95	17.654(14)	-0.003
	80000(31)	630.7(8)		22.197(14)	
4.15	30000(6)	294.6(3)		3.096(4)	
	35000(8)	328.1(2)		4.627(7)	
	40000(32)	362.8(7)		6.255(12)	
	45000(6)	397.2(3)		7.931(7)	
	50000(11)	431.9(4)		9.683(7)	
	55000(10)	467.3(6)		11.561(9)	
	60000(48)	503.3(6)		13.510(10)	
	65000(17)	540.7(6)		15.548(12)	
	80000(43)	654.4(9)	-2.26	22.194(18)	-0.035
	90000(62)	735.4(6)		27.013(14)	
4.26	35000(16)	349.3(6)		4.770(8)	
	40000(15)	383.7(6)		6.353(9)	
	45000(25)	418.7(4)		8.043(7)	
	50000(17)	454.4(7)		9.796(12)	
	55000(17)	491.1(6)		11.656(10)	
4.37	30000(7)	332.3(4)		3.338(8)	
	35000(7)	368.1(3)		4.863(6)	
	40000(8)	404.0(4)		6.456(8)	
	45000(11)	440.5(4)		8.128(9)	
	50000(10)	477.3(3)		9.894(6)	
	55000(13)	515.2(6)		11.759(8)	
	60000(10)	553.2(4)		13.684(6)	
4.48	40000(7)	425.2(3)		6.553(6)	
	45000(8)	463.2(4)		8.247(5)	
	50000(6)	501.2(5)		9.996(8)	
	55000(10)	539.1(4)		11.831(5)	
	60000(7)	579.2(4)		13.771(7)	
	65000(12)	619.7(8)		15.804(12)	
	70000(82)	660.5(10)		17.904(18)	

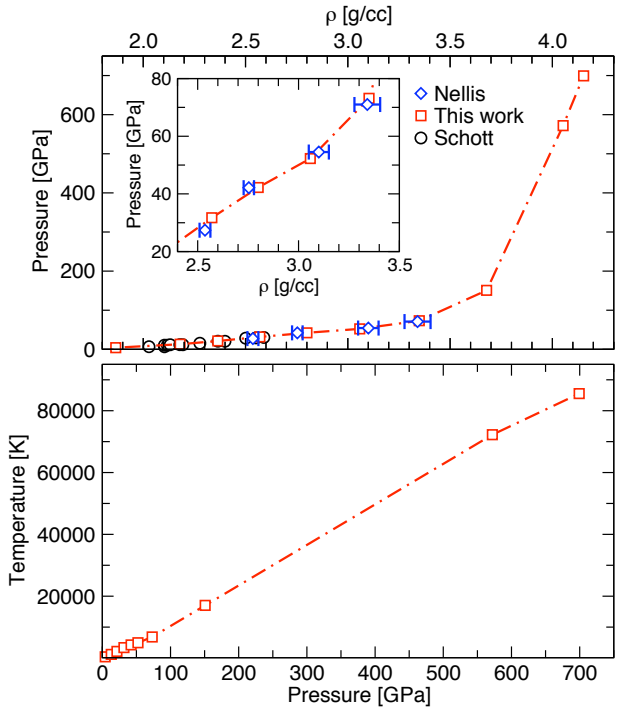

FIG. 1. P-ρ (top) and T-P (bottom) Hugoniots computed using the initial conditions of Nellis *et al.* [20]. The inset shows a closer comparison with the experimental data of Nellis *et al.* [20] and Schott *et al.* [35].

In addition, close inspection of Fig. 1 revels a subtle deflection in the computed Hugoniot near 2.570 g/cc and 41.6 GPa, which is consistent with the experimental measurements. As discussed in more detail in the following section, this region coincides with the onset of a significant fraction of molecular dissociation and the transformation to a complex mixture consisting of a variety of species, including CO_2, CO, O_2, and O.

To provide comparison with possible future experimental measurements, we have calculated the Hugoniot curves for several other initial densities and temperatures. As shown in Fig. 2, subtle changes in the starting density allows one to investigate considerably different regions of the high-P and T liquid. This is important if one is to understand the properties of liquid carbon dioxide over a wide range of extreme conditions. Moreover, it allows one to probe different areas along any liquid phase boundaries that may be present. Although not shown in Fig. 2, moderate variations in the initial temperature (+/- 200 K) do not lead to significant differences in the computed Hugoniots. By utilizing modern experimental approaches, such as those based on lasers [22] or pulse power techniques [21], it should be possible to realize the high-P and T regimes explored in these calculations and to directly verify the predicted Hugoniot data shown in Fig. 2.

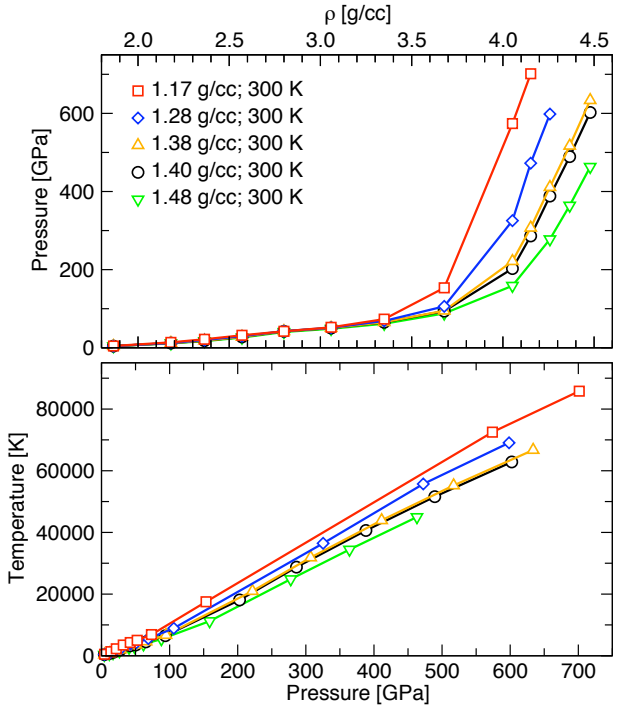

FIG. 2. P-ρ (top) and T-P (bottom) Hugoniots computed for several initial conditions.

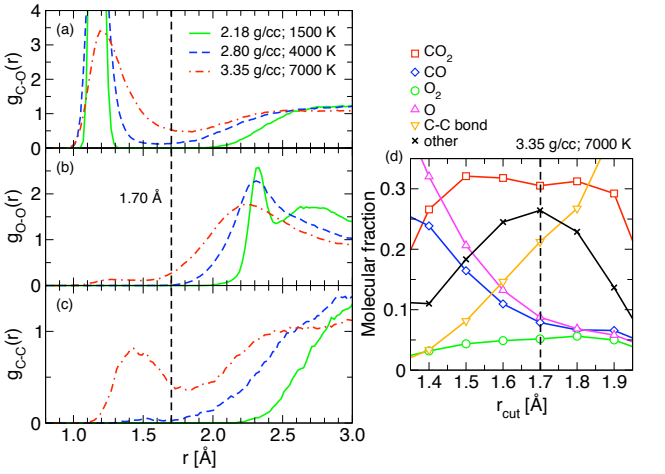

FIG. 3. Partial pair correlation functions of (a) C-O, (b) O-O, and (c) C-C atoms. The dashed line at 1.70Å indicates an approximation to the first minimum of each g(r). (d) Calculated average molecular fractions of several species (see text for definitions) as a function of the parameter r_{cut} at a CO_2 density of 3.35 g/cc and T = 7000 K. Here C-C indicates clusters containing C-C bonds.

B. Liquid structure and properties

In the following, the evolution of the fluid's structural properties along the Hugoniot (corresponding to ρ_0 = 1.172 g/cc and T_0 = 218.5 K) are described using two types of analysis: (i) by determining the types of species present in the liquid and calculating the average fractions of each species; and (ii) by determining the dynamical stability of each species by calculating their respective survival probabilities.

The identification of chemical species, or clusters, in a dense fluid is somewhat arbitrary and a wide variety of definitions have been proposed. We chose to use one based on a simple bond-length criteria. The precise definition is as follows: a cut-off radius (r_{cut}) is selected and used to construct a sphere of radius r_{cut} about each atom in the system. A molecular species is defined as a series of overlapping spheres (*i.e.* a CO_2 molecule would be defined as a sphere centered on a carbon atom that overlaps two spheres centered on oxygen atoms, where none of the three spheres overlap with those of any other atoms in the system). The number of each species is counted at each configuration in the FPMD trajectory. The amount of each species is then normalized by the total number of all detected species. This gives the final molecular fraction for each species detected over the entire simulation, where the sum of all fractions is equal to one. This analysis is sensitive to only one free parameter, r_{cut}. We have carefully chosen a cut-off radius based on the partial pair-correlation functions (see Fig. 3 (a), (b), and (c)). Covalent bonding occurs within the first-peak regime of g(r), thus, we wish to choose a value of r_{cut} that is near the first minimum. The dashed line shows a value of r_{cut} (1.70Å) that best approximates the first minimum of each g(r). Notice that the position of this minimum does not change significantly with density, and C-C and O-O bonding only appears at high density. Fig. 3 (d) shows the fractions of several species computed over a range of different of cut-off radii. A good choice for r_{cut} is one where the molecular fractions do not vary strongly for small changes in r_{cut}. We see that most of the molecular fractions plateau at $\sim$ 1.70 Å, the same distance that best coincides with the first minima in the pair correlation functions. Based on Fig. 3 we have chosen to use a cut-off of 1.70 Å for our analysis.

Using the aforementioned definition of a chemical species, we have computed the species fractions along the Hugoniot, shown in Fig. 4 (top). Each point corresponds to the computed fraction of the respective species averaged over the final 5 ps of a FPMD simulation at the given pressure and density. For pressures above the previously discussed deflection point in the Hugoniot, the fraction of CO_2 molecules sharply decreases, which leads to the appearance of O_2, CO, atomic oxygen, and several larger compounds often containing carbon-carbon bonding. The fractions of these newly formed species continue to increase along the Hugoniot.

Although a number of different chemical species are formed upon dissociation of CO_2, it is important to note that the fluid is highly reactive, and many of the species identified at each MD time step have very short lifetimes. For a comprehensive description of the liquid structure, it is therefore necessary to perform a dynamical analysis

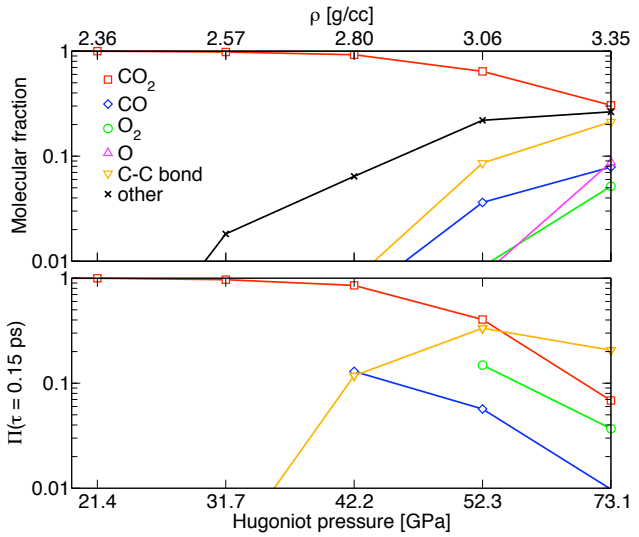

FIG. 4. (top) Average fractions of various species along the Hugoniot ($\rho_0 = 1.172$ g/cc, $T_0 = 218.5$ K) computed as described in the text. (bottom) Survival probabilities of several molecular species along the Hugoniot using a time-constant of 0.15 ps. Here C-C refers to species containing C-C bonds, while the corresponding survival probability refers to the C-C bond alone, not the whole cluster.

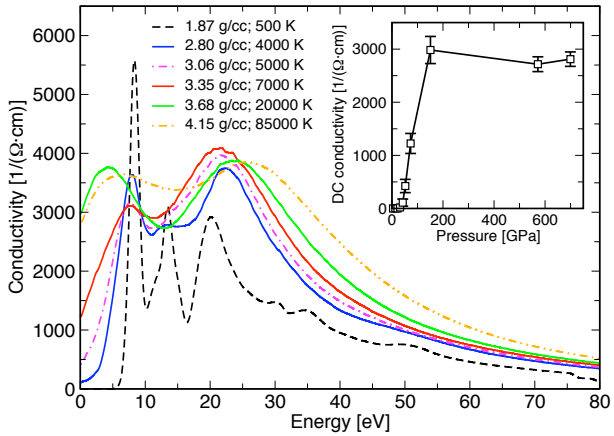

FIG. 5. Frequency dependent conductivity of CO_2 along the Hugoniot. (inset) DC conductivity as a function of pressure along the Hugoniot.

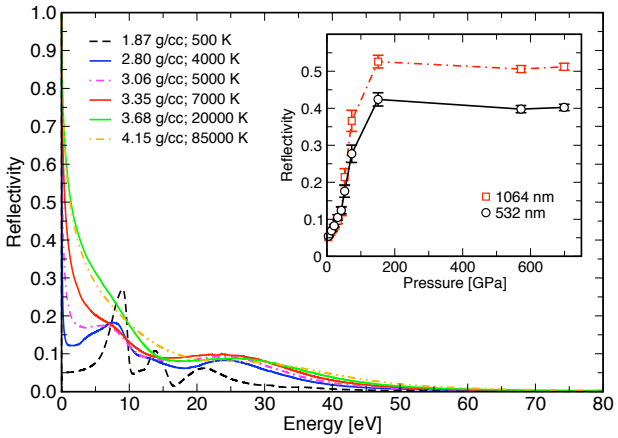

FIG. 6. Frequency dependence of the reflectivity of CO_2 along the Hugoniot. (inset) Reflectivity at 1064 nm and 532 nm as a function of pressure along the Hugoniot.

that quantifies the stability the different species in the fluid. To achieve this, we have computed the survival probabilities (denoted $\Pi(\tau)$) of notable molecular species along the Hugoniot, where τ is a time parameter. The survival probability of a given cluster is defined as the probability that a cluster existing at time $t = 0$ will also exist at a time $t = \tau$ in the future. We have chosen a value of $\tau = 0.15$ ps to allow 10 CO_2 anti-symmetric stretches before gauging cluster stabilities. The analysis is not qualitatively affected by different choices of τ and has been used previously with success in describing liquid phase transitions in both hydrogen [36] and nitrogen [37]. The survival probabilities for several species are shown in Fig. 4 (bottom). Above the transition, the stability of CO_2 molecules decreases rapidly and although the fractions of CO and O_2 molecules continue to increase beyond the transition, they too become less stable at higher pressures and temperatures. However, the fraction of C-C bond containing compounds continues to increase along the Hugoniot and the C-C bonds themselves remain relatively stable. Eventually, the stability of CO_2 bonding becomes less than the C-C bonds, and C-C bonds become the most stable in the system. This suggests the possibility of C/O phase separation that could lead to the formation of nanodiamond-like structures.

C. Optical properties

Using the Kubo-Greenwood approach, we have calculated the electronic component of the conductivity and corresponding reflectivity of the fluid for points along the Hugoniot ($\rho_0 = 1.172$ g/cc, $T_0 = 218.5$ K). The DC conductivity along the Hugoniot becomes non-zero above 2.57 g/cc and 4000 K (see Fig. 5). Under these conditions, the conduction states are beginning to populate due to temperature and a pseudo gap is formed. The DC conductivity is finite, however, the system is far from Drude-like behavior due to the localized nature of the electronic states in the pseudo gap. The closing of the gap, combined with Fermi-Dirac electronic excitations results in the population of anti-bonding states. These states, in turn, promote the dissociation of CO_2 molecules and contributes to the decrease in slope of the Hugoniot near 2.80 g/cc.

At a density of 3.06 g/cc, the peak in the spectra at 12 eV disappears and the DC conductivity rapidly increases along the Hugoniot before reaching a plateau near 3.68 g/cc and 20000 K. Even under the very high tem-

peratures considered here ($\sim$ 85000 K), the conductivity does not exhibit a Drude form.

One of the experimental observables that is often readily available in laser-based shock experiments is the reflectivity. For CO_2, the calculated reflectivity (Fig. 6) shows a progression comparable to the DC conductivity. The reflectivity (at wavelengths of 1064 nm and 532 nm) increases gradually until 3.0 g/cc where it then increases sharply before plateauing above 3.68 g/cc.

IV. CONCLUSIONS

We have computed the Hugoniot of carbon dioxide up to 1 TPa, which is in excellent agreement with previous gas gun shock experiments that were able to achieve pressures of up to 70 GPa. Several Hugoniot curves with different initial states have been presented along with equation of state data for future comparison with experiments. We find a phase transition in the liquid near 2.570 g/cc and 41.6 GPa that corresponds to the dissociation of carbon dioxide molecules and formation of other molecular species. The structural properties and molecular composition of the liquid along the Hugoniot have been described using molecular fractions and survival probability analysis. Furthermore, we have presented calculations of the conductivity and reflectivity of liquid carbon dioxide along the Hugoniot. We find that the DC conductivity and the reflectivity both increase upon dissociation of the CO_2 molecules. The optical properties presented here can be used for direct comparison with future experimental measurements.

V. ACKNOWLEDGMENTS

This work was performed under the auspices of the U.S. Dept. of Energy at the LLNL under contract no. DE-AC52-07NA27344. B.B. and S.A.B. acknowledge support from NSERC, Killam Trusts and Acenet.

[1] V. Iota, C. Yoo, and H. Cynn, Science **283**, 1510 (1999).
[2] M. I. Eremets, A. Gavriliuk, I. Trojan, D. Dzivenko, and R. Boehler, Nature Materials **3**, 558 (2004).
[3] M. Ross, Nature **292**, 435 (1981).
[4] W. Hubbard, Science **214**, 145 (1981).
[5] L. Benedetti, J. Nguyen, W. Caldwell, H. Liu, M. Kruger, and R. Jeanloz, Science **286**, 100 (1999).
[6] S. Serra, C. Cavazzoni, G. Chiarotti, S. Scandolo, and E. Tosatti, Science **284**, 788 (1999).
[7] C. Yoo, H. Cynn, F. Gygi, G. Galli, V. Iota, M. Nicol, S. Carlson, D. Häusermann, and C. Mailhiot, Phys. Rev. Lett. **83**, 5527 (1999).
[8] O. Tschauner, H. Mao, and R. Hemley, Phys. Rev. Lett. **87**, 075701 (2001).
[9] C. Yoo, H. Kohlmann, H. Cynn, M. Nicol, V. Iota, and T. LeBihan, Phys. Rev. B **65**, 104103 (2002).
[10] S. Bonev, F. Gygi, T. Ogitsu, and G. Galli, Phys. Rev. Lett. **91**, 065501 (2003).
[11] V. Giordano, F. Datchi, and A. Dewaele, J. Chem. Phys. **125**, 054504 (2006).
[12] M. Santoro, F. Gorelli, R. Bini, G. Ruocco, S. Scandolo, and W. Crichton, Nature **441**, 857 (2006).
[13] V. Iota, C. Yoo, J. Klepeis, Z. Jenei, W. Evans, and H. Cynn, Nature Materials **6**, 34 (2007).
[14] V. Giordano and F. Datchi, Europhysics Letters **77**, 46002 (2007).
[15] J. Montoya, R. Rousseau, M. Santoro, F. Gorelli, and S. Scandolo, Phys. Rev. Lett. **100**, 163002 (2008).
[16] A. Sengupta and C. Yoo, Phys. Rev. B **80**, 014118 (2009).
[17] F. Datchi, V. Giordano, P. Munsch, and A. M. Saitta, Phys. Rev. Lett. **103**, 185701 (2009).
[18] A. Sengupta and C. Yoo, Phys. Rev. B **82**, 012105 (2010).
[19] F. Tassone, G. Chiarotti, R. Rousseau, S. Scandolo, and E. Tosatti, Chem. Phys. Chem. **6**, 1752 (2005).
[20] W. Nellis, A. Mitchell, F. Ree, M. Ross, N. Holmes, and R. Trainor, J. Chem. Phys. **95**, 5268 (1991).
[21] M. D. Knudson, D. L. Hanson, J. E. Bailey, C. A. Hall, J. R. Asay, and C. Deeney, Phys. Rev. B **69**, 144209 (2004).
[22] D. G. Hicks, T. R. Boehly, P. M. Celliers, J. H. Eggert, S. J. Moon, D. D. Meyerhofer, and G. W. Collins, Phys. Rev. B **79**, 014112 (2009).
[23] M. D. Knudson and M. P. Desjarlais, Phys. Rev. Lett. **103**, 225501 (2009).
[24] A. A. Correa, L. X. Benedict, D. A. Young, E. Schwegler, and S. A. Bonev, Phys. Rev. B **78**, 024101 (2008).
[25] T. J. Lenosky, S. R. Bickham, J. D. Kress, and L. A. Collins, Phys. Rev. B **61**, 1 (2000).
[26] B. Militzer and D. M. Ceperley, Phys. Rev. Lett. **85**, 1890 (2000).
[27] M. P. Desjarlais, Phys. Rev. B **68**, 064204 (2003).
[28] S. A. Bonev, B. Militzer, and G. Galli, Phys. Rev. B **69**, 014101 (2004).
[29] A. B. Belonoshko, A. Rosengren, N. V. Skorodumova, S. Bastea, and B. Johansson, J. Chem. Phys. **122**, 124503 (2005).
[30] W. Kohn and L. J. Sham, Phys. Rev. **140**, A1133 (1965).
[31] J. P. Perdew, K. Burke, and M. Ernzerhof, Phys. Rev. Lett. **77**, 3865 (1996).
[32] G. Kresse and J. Hafner, Phys. Rev. B **47**, 558 (1993); Comp. Mat. Sci. **6**, 15 (1996).
[33] B. Holst, R. Redmer, and M. P. Desjarlais, Phys. Rev. B **77**, 184201 (2008).
[34] J. D. K. D. A. Horner and L. A. Collins, Phys. Rev. B **77**, 064102 (2008).
[35] G. Schott, High Press. Phys. **6**, 187 (1991).
[36] I. Tamblyn and S. Bonev, Phys. Rev. Lett. **104**, 065702 (2010).
[37] B. Boates and S. Bonev, Phys. Rev. Lett. **102**, 015701 (2009).